Dictyostelium myosin II mechanochemistry promotes active behavior of the cortex on long time scales

Kristine D. Girard*, Scot C. Kuo†, and Douglas N. Robinson*‡

Departments of *Cell Biology and †Biomedical Engineering, The Johns Hopkins University School of Medicine, 725 North Wolfe Street, Baltimore, MD 21205

Edited by Thomas D. Pollard, Yale University, New Haven, CT, and approved December 23, 2005 (received for review October 7, 2005)

Cell cortices rearrange dynamically to complete cytokinesis, crawl in response to chemoattractant, build tissues, and make neuronal connections. Highly enriched in the cell cortex, actin, myosin II, and actin crosslinkers facilitate cortical movements. Because cortical behavior is the consequence of nanoscale biochemical events, it is essential to probe the cortex at this level. Here, we use high-resolution laser-based particle tracking to examine how myosin II mechanochemistry and dynacortin-mediated actin crosslinking control cortex dynamics in *Dictyostelium*. Consistent with its low duty ratio, myosin II does not directly drive active bead motility. Instead, myosin II and dynacortin antagonistically regulate other active processes in the living cortex.

cell mechanics | dynacortin | laser-based particle tracking | nanoscale

Mediated by an actin filament network, the myosin II motor protein has a central role in many cellular shape changes (1–3) and uses energy from ATP hydrolysis to mechanically move and slide actin filaments (4). However, unlike the highly ordered structure of muscle, nonmuscle myosin II usually works on a less-ordered array of short cortical actin filaments. During its mechanochemical cycle, myosin II tightly binds actin and swings its lever arm, moving the filament ≈8 nm (for *Dictyostelium* myosin II) (5) (Fig. 1*A*). The maximum velocity with which the motor moves an actin filament is limited by the strongly bound-state time ($\tau_s = 1/k_{\text{ADP-release}}$; $\tau_s = 2.4$ ms for *Dictyostelium* myosin II) and the step size of the motor. Importantly, the motor is not simply a dynamic crosslinker; rather it changes the actin network by generating force to slide the actin filaments.

Various myosin II isoforms differ dramatically in their duty ratios and thick-filament assembly states. Muscle myosin IIs are tuned so that each thick filament has tens of heads associating with the actin filaments, allowing the sarcomere to contract and maintain tension (6, 7). In contrast, mammalian nonmuscle myosin IIs assemble into small minithick filaments and have a range of duty ratios so that as few as one or two to tens of motor heads per thick filament engage actin at a time, depending on the isoform (nmhcII-A, -B, or -C) (8–13). With so few heads associated, low duty-ratio motors may not sustain tension as readily or slide actin filaments significant distances as expected for muscle myosin II.

Expressing many of the same cytoskeletal proteins, *Dictyostelium* cells behave similarly to higher eukaryotic cells, such as human neutrophils, but offer exquisite genetic control over the proteins. *Dictyostelium* are also relatively mechanically simple because they do not appear to have stress fibers or intermediate filaments. Similar to mammalian nmhcII-A, *Dictyostelium* myosin II has a low duty ratio and thick-filament assembly state that allows as few as one head per thick filament to engage actin at a time (5, 14, 15). We demonstrate here that *Dictyostelium* myosin II mechanochemistry promotes nonmyosin II-driven cortical rearrangements.

Results

Experimental Design. Using high-resolution, laser-based particle tracking (LPT, Fig. 1*B*) (16–18), we examined the time scale-dependent behavior of the *Dictyostelium* cell cortex where most of the functional myosin II resides (Fig. 1 *C* and *D*) (19, 20). In the LPT assay, carboxylated polystyrene beads were attached to the surface of the cell. Even though the beads were topologically on the extracellular surface, our measurements were dominated by the actin cytoskeleton. Latrunculin treatment, which depolymerizes filamentous actin, increased the magnitude of the mean-squared displacements (MSDs) of the beads by nearly 10-fold, confirming our prior results (Fig. 6*A*, which is published as supporting information on the PNAS web site) (21). In *Dictyostelium*, cortical actin is largely randomly oriented, and the overall average actin filament length is ≈0.2 μm (22, 23). By using 0.7-μm-diameter beads, we ensured that the bead samples the average behaviors of many filaments. To demonstrate that the beads did not trigger cytoskeletal recruitment, we examined the surface of cells expressing coronin-GFP (a marker for actin), GFP-dynacortin, or GFP-myosin II. At the level of fluorescence microscopy, none of the proteins appeared to be recruited to the bead (Fig. 1*C*). Although it is possible that different locations in the cortex have different characteristics, we have yet to detect any correlation between bead behavior and cortical location.

To analyze its role, we perturbed myosin II genetically, using gene deletion, RNA interference, and site-directed mutagenesis. To verify the genetic strains, we performed Western analysis, probing for myosin II and dynacortin expression (Fig. 1*E*). Myosin II and dynacortin were silenced by myosin II and dynacortin hairpin constructs, respectively, and neither protein was detectable in wild-type (wt) cells carrying the hairpin. Dynacortin was only weakly detectable in *myoII*:dynhp cells.

Myosin II Specifies, but Does Not Drive, Active Particle Behaviors. In living cells, different motile (active) processes are likely to occur on distinct time scales. These active processes include energy-dependent activities such as motor-driven or polymer-driven motility and cell crawling. The cytoskeleton and the plasma membrane also contribute to passive subdiffusive cellular properties. To distinguish active from passive behaviors, statistical analysis of particle motions is required. The power-law behavior of the MSDs ($\text{MSD} \propto \tau^{\gamma}$, where γ is the power law and τ is the correlation time) separate active (superdiffusive, $\gamma > 1$) and passive (subdiffusive, $\gamma < 1$) behaviors. At each time scale, larger magnitudes of MSDs also indicate greater freedom of motion and may indicate changes in resistance or molecular binding. As shown below, active processes occur on different time scales. Remarkably, only two classes of active behaviors were observed: subsecond active (SSA) (active at $\tau > 200$ ms) and subsecond passive (SSP) (active at $\tau > 1$ s).

Detrending algorithms remove long-distance motions that are probably caused by cell crawling. The SSP class of beads fluctuated along a path that was relatively straight and detrending

Conflict of interest statement: No conflicts declared.

This paper was submitted directly (Track II) to the PNAS office.

Abbreviations: SSP, subsecond passive; SSA, subsecond active; LPT, laser-based particle tracking; MSD, mean-squared displacement; wt, wild type.

‡To whom correspondence should be addressed. E-mail: dnr@jhmi.edu.

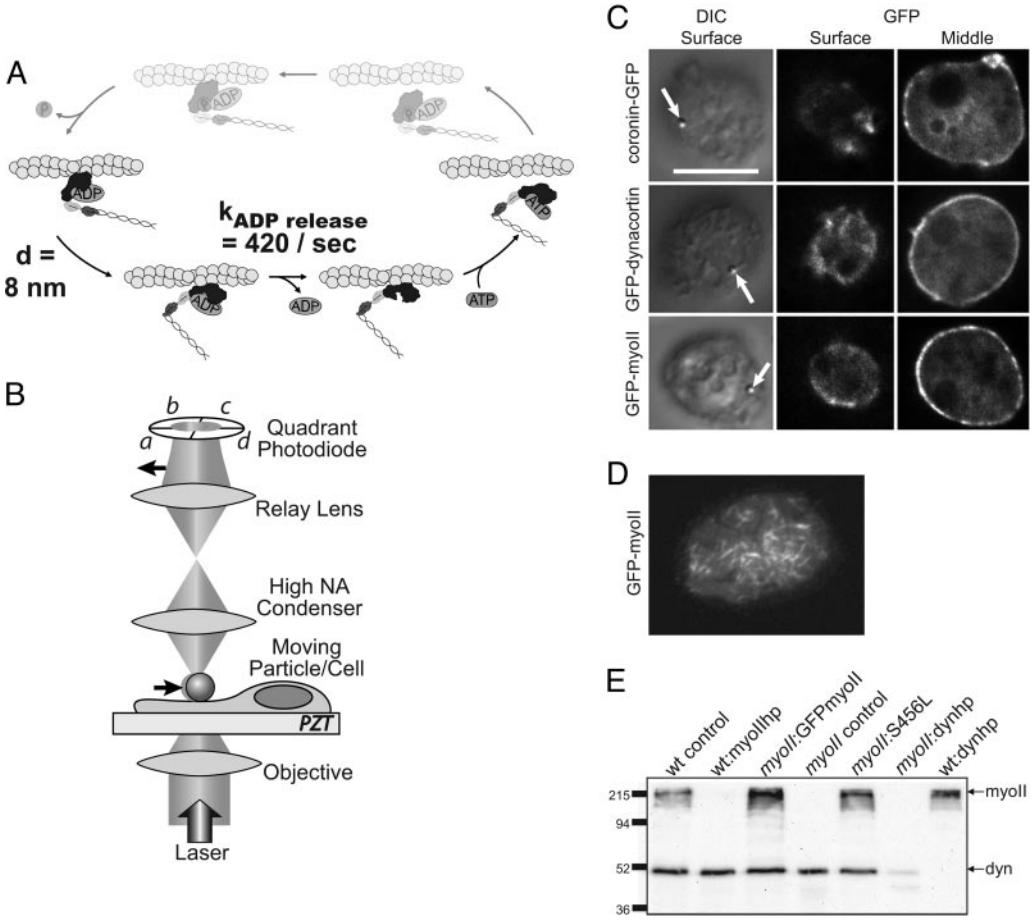

Fig. 1. LPT system for measuring cortical mechanics of *Dictyostelium discoideum*. (*A*) Myosin-II ATP hydrolysis cycle. The rate-limiting step for motility is $k_{ADP\text{-}release}$, which is 420 s^{-1}, yielding a strongly bound-state time τ_s of 2.4 ms (5). (*B*) The LPT system uses a low-power laser that focuses on a 0.7 μm-carboxylated polystyrene bead attached to the surface of a *Dictyostelium* cell. Bead motions deflect the laser beam, which is relayed to a quadrant photodiode detector. (*C*) Differential interference contrast microscopy (DIC) and fluorescence imaging of coronin-GFP (46), GFP-dynacortin (28), and GFP-myosin II (44) shows that the bead (*Left*, arrows) does not recruit coronin, dynacortin, or myosin II. Surface (*Center*) and middle (*Right*) sections of deconvolved images are shown for comparison. (Scale bar, 10 μm.) (*D*) Total internal reflection fluorescence microscopy demonstrates that myosin II thick filaments are assembled in the cortex. (*E*) Western analysis using anti-myosin II monoclonal and anti-dynacortin polyclonal antibodies of cells expressing various myosin II and dynacortin constructs.

algorithms readily removed the long-distance excursions (Fig. 2 *A* and *B*). The MSDs of the SSP class displayed subdiffusive behavior ($\gamma < 1$ when $\tau < \approx 1$ s, Fig. 2*C*) before detrending and were subdiffusive across the entire time-scale range after detrending (Fig. 2*D*). The SSA class of beads followed meandering paths, and detrending failed to collapse the trajectories, suggesting that the bead was undergoing active motility (Fig. 2 *F* and *G*). Not only did linear detrending fail to collapse the trajectories, the magnitude of MSDs on fast time scales ($\tau < 100$ ms) was ≈2-fold lower than the SSP class, suggesting a different mode of coupling to an active cytoskeleton (Fig. 2 *D* and *I*). The superdiffusive behavior ($\gamma > 1$) of the SSA class began ≈200–300 ms, which is ≈100-fold slower than the strongly bound state time (2.4 ms) of *Dictyostelium* myosin II (Fig. 2 *H* and *I*). Thus, it is unlikely that myosin II-mediated transport directly drives motility of the beads in the SSA class.

To classify the bead behaviors numerically, we calculated the local power laws of MSDs at $\tau = 1$ s and present frequency histograms for each genotype (Fig. 3). About 75% of the particles on wt cells (wt control) and complemented myosin II mutant cells (*myoII*:GFPmyosin II) showed superdiffusive ($\gamma > 1$) behavior at $\tau = 1$ s (the SSA class), whereas the remaining (25%) beads were subdiffusive ($\gamma < 1$) (the SSP class) (Figs. 2 *E* and *J* and 3 *A* and *B*). Cells devoid of myosin II, either by gene deletion (*myoII* control) or RNA interference (wt:myoIIhp), had only ≈30% of the particles in the SSA class, whereas the remaining (70%) particles were in the SSP class (Fig. 3 *C* and *D*). These results indicate that myosin II promotes, but is not essential for, active cortical behavior on the subsecond time scale (Fig. 7, which is published as supporting information on the PNAS web site).

Active Particle Behavior Requires Myosin II Mechanochemistry. To verify that the frequency of the SSA class is caused by myosin II mechanochemistry, we examined cells expressing mutant myosin II, S456L, which has uncoupled mechanochemical transduction (5, 24). S456L partially rescues the cytokinesis and developmental defects of myosin II mutant cells. *In vitro*, S456L has a 10-fold slower actin-sliding velocity caused by a shorter step size (1/4 wt) and slower ADP-release rate (1/3 wt) (5). As compared with the myosin II mutant, the uncoupler mutant partially increased the fraction of beads in the SSA class. Because wt myosin II has a much larger effect, its mechanochemistry is required to fully promote active cortical processes (SSA; Fig. 3*G*). Further, the altered kinetic tuning of S456L does not shift the time scale of the active motility of the SSA class when compared with myosin II mutants and wt cells, providing further evidence that myosin II does not directly drive the active behavior of the SSA class (Fig. 7).

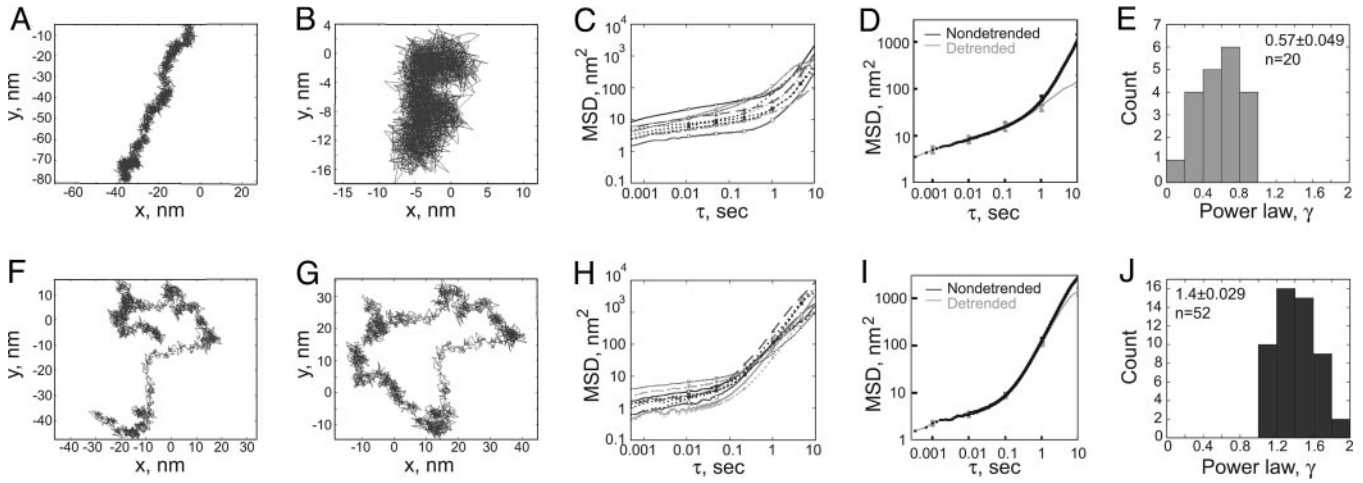

Fig. 2. Beads on wt cortices show time scale-dependent subdiffusive and superdiffusive behaviors. (*A*) An example of a bead trace that showed largely diffusive behavior directed along a linear path over a 20-s interval. (*B*) Bead path in *A* after linear detrending to remove long-distance motility that probably results from cell crawling. (*C*) Plot of nondetrended MSDs vs. correlation time τ for 10 beads, showing SSP behavior for time scales shorter than ≈1 s. (*D*) Average MSD plots for nondetrended and detrended trajectories for the class of beads that show SSP behavior. (*E*) Distribution of power laws calculated from the detrended data at $\tau = 1$ s by using a three-quarter-decade interval (from 0.4 to 2.4 s) for this class of bead behaviors. (*F*) An example of a bead path that showed SSA behavior. (*G*) Bead path in *F* after linear detrending. (*H*) Plot of nondetrended MSDs vs. τ for 10 beads showing SSA behavior on time scales more than ≈200 ms. (*I*) Average MSD plots for nondetrended and detrended trajectories for the class of beads that show largely superdiffusive behavior on time scales >200 ms. (*J*) Distribution of power laws calculated from the detrended data at $\tau = 1$ s by using a three-quarter-decade interval (from 0.4 to 2.4 s) for this class of beads.

Myosin II and Dynacortin Control the Frequency of Active Particle Behavior. To contrast the motor with an actin crosslinker, we examined cells depleted of dynacortin. Dynacortin and myosin II have opposing roles in controlling cytokinesis dynamics and morphology (21, 25). In wt cells, removal of dynacortin did not affect the frequency of the SSA class (Fig. 3*E*). However, in myosin II mutant cells, removal of dynacortin increased the frequency of the SSA class, producing a clearly bimodal distribution with about half of the beads experiencing each type of behavior (Fig. 3*F*). Because dynacortin is an actin crosslinker, its biochemical activity suggests a mechanical role in modulating the frequency with which the SSA behavior occurs, even in the absence of myosin II mechanochemistry (Fig. 3*H*).

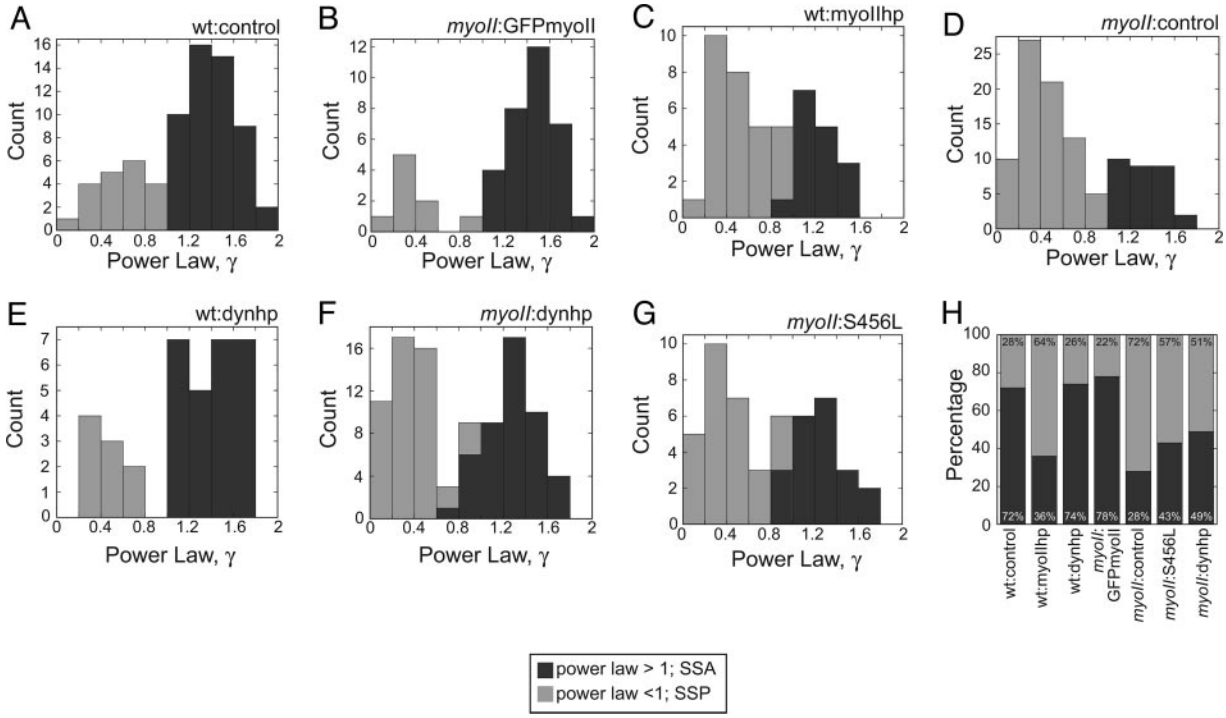

Fig. 3. All genotypes show similar types of SSA and SSP bead behaviors but differ in the frequency of each type of behavior. (*A–G*) Histograms of distributions of power law, γ, at $\tau = 1$ s for detrended data. Any bead that had $\gamma > 1$ at any point was shaded dark gray, regardless of its γ at precisely $\tau = 1$ s. (*A*) wt control, $n = 72$. (*B*) *myoII*:GFPmyoII, $n = 41$. (*C*) wt:myoIIhp, $n = 44$. (*D*) *myoII* control, $n = 106$. (*E*) wt:dynhp, $n = 35$. (*F*) *myoII*:dynhp, $n = 96$. (*G*) *myoII*:S456L, $n = 49$. (*H*) Frequency histogram representing the fraction of beads in each class for each genotype.

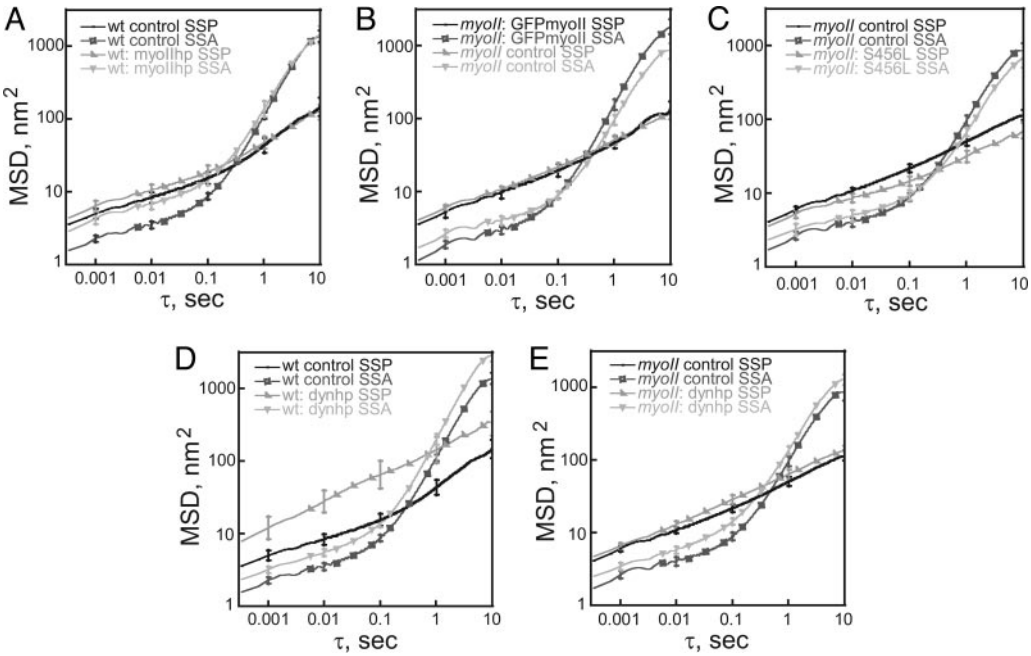

Fig. 4. Spectra of MSD magnitudes for two bead classes demonstrate that dynacortin has the largest impact on the SSP class. (*A*) wt control vs. wt:myoIIhp. (*B*) *myoII*:GFPmyoII vs. *myoII* control. (*C*) *myoII* control vs. *myoII*:S456L. (*D*) wt control vs. wt dynhp. (*E*) *myoII* control vs. *myoII*:dynhp. Error bars are SEMs. The *n* values are as shown in the Fig. 3 legend.

Complex Interactions Between Myosin II and Dynacortin. Cortical rearrangements depend on both active and passive features of the living cortex. By segregating the bead behaviors, we can determine how myosin II and dynacortin control the magnitudes of the MSD spectra for both SSA and SSP classes (Figs. 4, 5, and 7). For the SSA and SSP classes, neither type of myosin II had a major effect on the magnitude of the MSDs (Figs. 4 *A–C* and 7 and Table 1, which is published as supporting information on the PNAS web site). Similarly, low concentrations (25 μM) of blebbistatin, an inhibitor of myosin II (26), weakly phenocopied the myosin II spectra (Fig. 6*F*). Higher concentrations of blebbistatin showed off-target effects in myosin II mutant cells, indicating nonspecificity (data not shown) (27). However, at 25 μM, blebbistatin did not alter the frequency distribution of SSP and SSA behaviors, suggesting that its inhibition is only partial. With its 2.4-ms τ_s, the wt myosin II motor domain remains unbound across most of the spectra so that it has only small effects on the SSA and SSP class magnitudes.

In contrast, dynacortin has a large (≈5-fold) effect on the magnitude of SSP bead spectra with little effect on the SSA bead population in a wt background (Figs. 4*D* and 7 and Table 1). In the myosin II mutant background, dynacortin had only small effects for both bead classes (Fig. 4*E* and Table 1). Thus, removal of dynacortin increased the magnitudes of the MSDs of the SSP class, indicating that its absence promotes a greater freedom of bead motion. However, dynacortin's effect depends on whether myosin II is present, indicating complex interactions between these proteins.

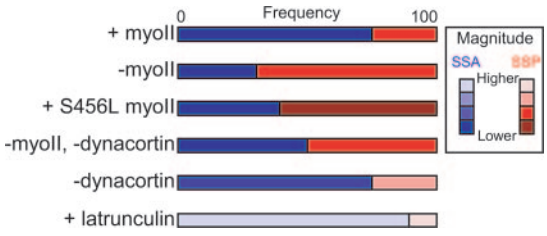

Fig. 5. Summary of myosin II and dynacortin control of active cortical processes. Frequency bars depict the fraction of particles in the SSA vs. SSP class for each protein and is drawn from data in Fig. 3*H*. Color shading reflects the magnitude of the MSDs. Blue bars represent the SSA class, and red bars represent the SSP class.

Discussion

Interpreting Extracellular Particle-Tracking Data. The objective of this article is to explore how myosin II and dynacortin control the activity of the cell cortex. These proteins are enriched in the thin cortex that surrounds the *Dictyostelium* cytoplasm (Fig. 1) (20, 28). To probe this thin cortical layer, the particles had to be applied to the external surface of the cell, relying on indirect coupling between the bead and the underlying actin network through the plasma membrane and its constituent lipids and proteins. The presence of two distinct classes of bead behaviors (SSA and SSP) suggests that there are primarily two modes of coupling, which are similar between all mutants studied here. Although the nature of these coupling modes is not yet known, they may represent differences in the cytoskeletal network, cytoskeleton-membrane domains, or cytoskeleton-membrane linkages. However, subtle changes in bead coupling cannot give rise to motile behaviors and explain our data. Yet, the largest effects of myosin II and dynacortin are in regulating the frequency with which SSA and SSP behaviors are observed. Because myosin II and dynacortin have distinct biochemical activities on the actin cytoskeleton, we propose that they regulate the two classes of bead behaviors indirectly by modulating the mechanical properties of the actin network.

Myosin II Mechanochemistry Promotes Active Cortical Behavior. Myosin II mechanochemistry facilitates the SSA class of behaviors, indicating that myosin II-driven flow of actin filaments is critical for wt cortical dynamics. This actin flow may create local cortical microdomains that are characterized by either SSA- or SSP-type behavior. We propose that wt myosin II mechanochemistry may reduce filament entanglements in microregions of

the cortex. *In vitro*, filament entanglements contribute to elastic behavior of purified actin networks (29), and muscle myosin II mechanochemistry can reduce the lifetimes of these entanglements, lowering the viscoelastic moduli of the networks (30). Although from muscle, the myosin II used in that study was assembled into artificially small filaments. From its duty ratio, only one or two heads per thick filament would have interacted with actin at a time, similar to native *Dictyostelium* myosin II. Removal of dynacortin from myosin II mutants also increases the frequency of the SSA behavior. If crosslinking increases the lifetimes of entanglements, dynacortin may mechanically antagonize the effect of myosin II mechanochemistry on the network.

It is unknown what directly drives the active (SSA class) bead motility (31, 32). Because latrunculin treatment did not remove the active behavior (see upturn in Fig. 6*A*), neither myosin II mechanochemistry nor actin dynamics are likely to drive the active behavior. Microtubule-based motility has been implicated for similar types of superdiffusive behavior (32). Because microtubules and motors such as dynein and Ddkin5 localize to the *Dictyostelium* cortex, these enzymes may modulate cortical anchoring of the microtubules (33, 34). These proteins may then drive the SSA class of motility by pulling microtubules through the actin cortex. In this case, the frequency of SSA behavior may be determined by the episodic encounters with microtubules, particularly if microtubule motility is retarded by cortical entanglements. Additionally, the actin network is an integral part of the force balance that centers the centrosome, which defines the cell center (34, 35).

Other studies implicate myosin II in controlling the mechanical nature of the cell. From magnetic twisting rheometry, myosin II appears to increase cytoplasmic fluidity of a related amoeba, *Entamoeba histolytica* (36). *Dictyostelium* myosin II mutants appear to have greater mechanical resistance as measured by micropipette aspiration and magnetic rheometry (37, 38), whereas other studies indicate that myosin II mutants have lower cortical tension (39, 40). Thus, myosin II contributes to the passive mechanics of the cell in many ways; however, our study separates myosin II's roles in active and passive behaviors of the cell cortex.

Our results are important for understanding how myosin II isoforms and actin crosslinkers contribute to cell shape changes such as cytokinesis. In cytokinesis, myosin II opposes dynacortin in controlling furrow thinning dynamics, a process inextricably linked to cell mechanics (25). During cytokinesis, myosin II mechanochemistry may promote contractility by increasing the flow of the actin network, perhaps by promoting force-dependent uncrosslinking by the actin crosslinking proteins. *In vitro*, myosin II can break actin filaments, pull filaments from crosslinked actin bundles, and increase the flow of actin filaments (30, 41, 42). As significant concentrations of myosin II remain in the cortex of the emerging daughter cells, globally distributed myosin II may also promote active cortical behavior, which might help facilitate cleavage furrow thinning (20). Similarly, myosin II activity is required for normal actin polymer turnover during mammalian cytokinesis (43).

Conclusions

Using carefully controlled genetically manipulated strains, we detected nanoscale properties of the living cortex that depend on the molecular properties of a single motor and actin crosslinker. Specifically, myosin II mechanochemistry promoted other non-myosin II-driven active cortical behaviors. We anticipate that the concept that nonmuscle myosin II increases the active nature of the cortex will be generalizable to many types of nonmuscle cells. However, the kinetic tuning (duty ratio) and the specific macromolecular assembly (thick filament size) of each myosin II isoform may prove to be a critical determinant of how each myosin II contributes to active cellular behaviors. Overall, this study reveals that myosin II mechanochemistry and actin crosslinking define the fundamental nature of an active living cortex.

Materials and Methods

Constructs and Strains. The myosin II (*mhcA*) hairpin construct (myoIIhp:pLD1A15SN) was generated from bases 1771–2731 for the antisense strand and bases 2129–2731 for the sense strand. These fragments were subcloned into pLD1A15SN, yielding myoIIhp:pLD1A15SN. This plasmid was transformed into *Dictyostelium* wt (Ax-3: Rep orf+7-3) cells and selected by using 15 μg/ml G418 (28). The dynhp:pLD1 construct has been described (21). Control cells were transformed with the empty pLD1A15SN vector. The *mhcA* (*myoII*) deletion mutant used was HS1 (19). *myoII* control, *myoII*:GFPmyoII, and *myoII*:S456L cells were generated by transforming HS1 cells with respective plasmids (5, 28, 44).

LPT. To measure the activity of living cell cortices, we used high-resolution LPT as described (21), but modified to incorporate longer time-scale information. Cells were plated on glass coverslips. Beads (0.7 μm) were tracked for 11 1-s intervals and an additional 20-s interval, which provided an additional decade of time-resolved information. For drug-treated cells, 25-μM blebbistatin (26) or 7.5-μM latrunculin B was added to the cells along with the polystyrene beads (21). Control cells were treated with the same concentration of DMSO, the solvent for blebbistatin and latrunculin B.

To study the bead behaviors, detrended and nondetrended bead fluctuations were compared (45) (Fig. 2). Bead behaviors were sorted into two groups in two independent ways. In the first numerical approach, the power law γ was calculated for each bead from the detrended data, using a three-quarter-decade window. Any bead trace that crossed over to $\gamma > 1$ at any point were put into one group (SSA class), and a second group (SSP class) was made up of beads that failed to cross over to $\gamma > 1$. In the second qualitative approach, bead paths before and after detrending were visually inspected. Those paths that appeared to detrend well were put into a group and those that did not appear to detrend well were put into a second group. The two approaches were conducted simultaneously and were blinded to each other. Both approaches gave nearly identical groupings with the exception of less than $\approx$10% of the bead tracks for all genotypes. The numerical approach was ultimately used to categorize the bead behaviors. Additionally, without sorting, the average (mean $\pm$ SEM) MSD spectra are presented for pooled data for each genotype and pharmacological treatment (Fig. 6).

Because data sets were not consistently lognormal, we computed statistics by assuming both lognormal and normal distributions. None of our conclusions differ in the two analyses. All means, SEMs, and statistical tests presented were calculated by assuming lognormal distributions with logarithmically transformed data.

Fluorescence Imaging. Cells expressing coronin-GFP (46), GFP-dynacortin (28), or GFP-myosin II (44) were plated in 1$\times$ PB buffer (20 mM Na_2HPO_4/20 mM NaH_2PO_4, pH 6.9), and 0.7-μm carboxylated polystyrene beads were allowed to adhere as in the LPT assay. We imaged the top surface by using differential interference contrast microscopy. For fluorescence imaging, cells were optically sectioned by using 0.38-μm steps and 20-ms exposure time, and image stacks were deconvolved by using the METAMORPH 3D-deconvolution module. The bottom surface was imaged by using total internal reflection fluorescence microscopy (TIRF) illumination. All imaging was performed with an Olympus IX81 epifluorescence and TIRF microscope equipped with a $\times$60 (numerical aperture 1.45) objective and a $\times$1.6 optivar. Images were collected with

METAMORPH (Universal Imaging, Downingtown, PA) and processed with Adobe Systems (San Jose, CA) PHOTOSHOP.

Western Immunodetection. To assess the amount of protein in each strain, Western analysis was performed by using horseradish peroxidase-conjugated donkey anti-rabbit secondary antibodies (Pierce), rabbit anti-dynacortin polyclonal antibodies (28), goat anti-mouse secondary antibodies (Pierce), and mouse anti-myosin II mAbs.

We thank the Spudich laboratory (Stanford University, Palo Alto, CA) for myosin II mutants; Ron Rock (University of Chicago), Pablo Iglesias (The Johns Hopkins University), Laura Schmidt (University of Chicago), Wendy Zhang (University of Chicago), John Crocker (University of Pennsylvania, Philadelphia), and members of D.N.R.'s laboratory for helpful discussions; and two anonymous reviewers for helpful comments on the manuscript. This work was supported by a Beckman Young Investigator Award (to D.N.R.) and National Institutes of Health Grants R01 GM066817 (to D.N.R.) and R01 GM59285 (to S.C.K.).

1. Koehl, G. & McNally, J. G. (2002) *Cell Biol. Int.* **26,** 287–296.
2. Brown, J. & Bridgman, P. C. (2003) *J. Histochem. Cytochem.* **51,** 421–428.
3. Robinson, D. N. & Spudich, J. A. (2004) *Curr. Opin. Cell Biol.* **16,** 182–188.
4. Spudich, J. A. (2001) *Nat. Rev. Mol. Cell Biol.* **2,** 387–392.
5. Murphy, C. T., Rock, R. S. & Spudich, J. A. (2001) *Nat. Cell Biol.* **3,** 311–315.
6. Pepe, F. A. & Drucker, B. (1979) *J. Mol. Biol.* **130,** 379–393.
7. Howard, J. (1997) *Nature* **389,** 561–567.
8. Niederman, R. & Pollard, T. D. (1975) *J. Cell Biol.* **67,** 72–92.
9. Verkhovsky, A. B. & Borisy, G. G. (1993) *J. Cell Biol.* **123,** 637–652.
10. Kovacs, M., Wang, F., Hu, A., Zhang, Y. & Sellers, J. R. (2003) *J. Biol. Chem.* **278,** 38132–38140.
11. Golomb, E., Ma, X., Jana, S. S., Preston, Y. A., Kawamoto, S., Shoham, N. G., Conti, M. A., Sellers, J. R. & Adelstein, R. S. (2004) *J. Biol. Chem.* **279,** 2800–2808.
12. Rosenfeld, S. S., Xing, J., Chen, L.-Q. & Sweeney, H. L. (2003) *J. Biol. Chem.* **278,** 27449–27455.
13. Wang, F., Kovacs, M., Hu, A., Limouze, J., Harvey, E. V. & Sellers, J. R. (2003) *J. Biol. Chem.* **278,** 27439–27448.
14. Ito, K., Liu, X., Katayama, E. & Uyeda, T. Q. P. (1999) *Biophys. J.* **76,** 985–992.
15. Mahajan, R. K. & Pardee, J. D. (1996) *Biochemistry* **35,** 15504–15514.
16. Yamada, S., Wirtz, D. & Kuo, S. C. (2000) *Biophys. J.* **78,** 1736–1747.
17. McGrath, J. L., Hartwig, J. H. & Kuo, S. C. (2000) *Biophys. J.* **79,** 3258–3266.
18. Mason, T. G., Ganesan, K., van Zanten, J. H., Wirtz, D. & Kuo, S. C. (1997) *Phys. Rev. Lett.* **79,** 3282–3285.
19. Ruppel, K. M., Uyeda, T. Q. P. & Spudich, J. A. (1994) *J. Biol. Chem.* **269,** 18773–18780.
20. Robinson, D. N., Cavet, G., Warrick, H. M. & Spudich, J. A. (2002) *BMC Cell Biol.* **3,** 4.
21. Girard, K. D., Chaney, C., Delannoy, M., Kuo, S. C. & Robinson, D. N. (2004) *EMBO J.* **23,** 1536–1546.
22. Medalia, O., Weber, I., Frangakis, A. S., Nicastro, D., Gerisch, G. & Baumeister, W. (2002) *Science* **298,** 1209–1213.
23. Podolski, J. L. & Steck, T. L. (1990) *J. Biol. Chem.* **265,** 1312–1318.
24. Ruppel, K. M. & Spudich, J. A. (1996) *Mol. Biol. Cell* **7,** 1123–1136.
25. Zhang, W. W. & Robinson, D. N. (2005) *Proc. Natl. Acad. Sci. USA* **102,** 7186–7191.
26. Straight, A. F., Cheung, A., Limouze, J., Chen, I., Westwood, N. J., Sellers, J. R. & Mitchison, T. J. (2003) *Science* **299,** 1743–1747.
27. Shu, S., Liu, X. & Korn, E. D. (2005) *Proc. Natl. Acad. Sci. USA* **102,** 1472–1477.
28. Robinson, D. N. & Spudich, J. A. (2000) *J. Cell Biol.* **150,** 823–838.
29. MacKintosh, F. C., Kas, J. & Janmey, P. A. (1995) *Phys. Rev. Lett.* **75,** 4425–4428.
30. Humphrey, D., Duggan, C., Saha, D., Smith, D. & Kas, J. (2002) *Nature* **416,** 413–416.
31. Lau, A. W. C., Hoffman, B. D., Davies, A., Crocker, J. C. & Lubensky, T. C. (2003) *Phys. Rev. Lett.* **91,** 198101.
32. Caspi, A., Granek, R. & Elbaum, M. (2000) *Phys. Rev. Lett.* **85,** 5655–5658.
33. Iwai, S., Ishiji, A., Mabuchi, I. & Sutoh, K. (2004) *J. Biol. Chem.* **279,** 4696–4704.
34. Brito, D. A., Strauss, J., Magidson, V., Tikhonenko, I., Khodjakov, A. & Koonce, M. P. (2005) *Mol. Biol. Cell* **16,** 3334–3340.
35. Vallee, R. B. & Stehman, S. A. (2005) *Trends Cell Biol.* **15,** 288–294.
36. Marion, S., Guillen, N., Bacri, J.-C. & Wilhelm, C. (2005) *Eur. Biophys. J.* **34,** 262–272.
37. Feneberg, W., Westphal, M. & Sackmann, E. (2001) *Eur. Biophys. J.* **30,** 284–294.
38. Merkel, R., Simson, R., Simson, D. A., Hohenadl, M., Boulbitch, A., Wallraff, E. & Sackmann, E. (2000) *Biophys. J.* **79,** 707–719.
39. Pasternak, C., Spudich, J. A. & Elson, E. L. (1989) *Nature* **341,** 549–551.
40. Dai, J., Ting-Beall, H. P., Hockmuth, R. M., Sheetz, M. P. & Titus, M. A. (1999) *Biophys. J.* **77,** 1168–1176.
41. Kron, S. J. & Spudich, J. A. (1986) *Proc. Natl. Acad. Sci. USA* **83,** 6272–6276.
42. Prassler, J., Stocker, S., Marriott, G., Heidecker, M., Kellermann, J. & Gerisch, G. (1997) *Mol. Biol. Cell* **8,** 83–95.
43. Guha, M., Zhou, M. & Wang, Y.-l. (2005) *Curr. Biol.* **15,** 732–736.
44. Moores, S. L., Sabry, J. H. & Spudich, J. A. (1996) *Proc. Natl. Acad. Sci. USA* **93,** 443–446.
45. Kuo, S. C. & McGrath, J. L. (2000) *Nature* **407,** 1026–1029.
46. Maniak, M., Rauchenberger, R., Albrecht, R., Murphy, J. & Gerisch, G. (1995) *Cell* **83,** 915–924.

Table 1. Student's two-tailed *t*-test of MSDs of SSP class beads

	Correlation time, τ			
Strain 1 (*n*) vs. Strain 2 (*n*)	1 msec	10 msec	100 msec	1 sec
Wt control (20) vs. wt:dynhp (9)	$0.02 < P < 0.05$*	$P < 0.01$*	$P < 0.01$*	$0.01 < P < 0.02$*
Wt control (20) vs. wt:myoIIhp (28)	$P > 0.2$	$P > 0.2$	$P > 0.2$	$P > 0.2$
myoII control (76) vs. *myoII*:S456L (28)	$P > 0.2$	$0.1 < P < 0.2$	$0.02 < P < 0.05$*	$0.02 < P < 0.05$*
myoII control (76) vs. *myoII*:GFPmyoII (9)	$P > 0.2$	$P > 0.2$	$P > 0.2$	$P > 0.2$
myoII control (76) vs. *myoII*:dynhp (49)	$P > 0.2$	$P > 0.2$	$0.1 < P < 0.2$	$P > 0.2$

*Comparison is statistically significant.

Fig. 6. Composite of mean MSD spectra for each genotype and pharmacological treatment. Graphs reflect all beads tracked, regardless of grouping. (*A*) wt control + DMSO vs. wt control + latrunculin B. (*B*) wt control vs. wt:dynhp. (*C*) *myoII* control vs. *myoII*:dynhp. (*D*) wt control vs. wt:myoIIhp. (*E*) *myoII* control vs. *myoII*:GFPmyoII. (*F*) wt control + DMSO vs. wt control + 25 μM blebbistatin. (*G*) *myoII* control vs. *myoII*:S456L. Error bars are SEMs. *n* values for each genotype are provided in the Fig. 3 legend. For the remainder, wt control + DMSO, $n = 27$; wt control + latrunculin B, $n = 9$; wt control + blebbistatin, $n = 35$. Analysis is based on detrended data.

Fig. 7. The SSA class of bead behaviors is largely independent of myosin II or dynacortin activities, whereas dynacortin has a significant effect on the SSP class. (*A*) Graph displays MSD spectra from the SSP class from all strains. (*B*) Graph displays the MSD spectra for the SSA class from all strains.

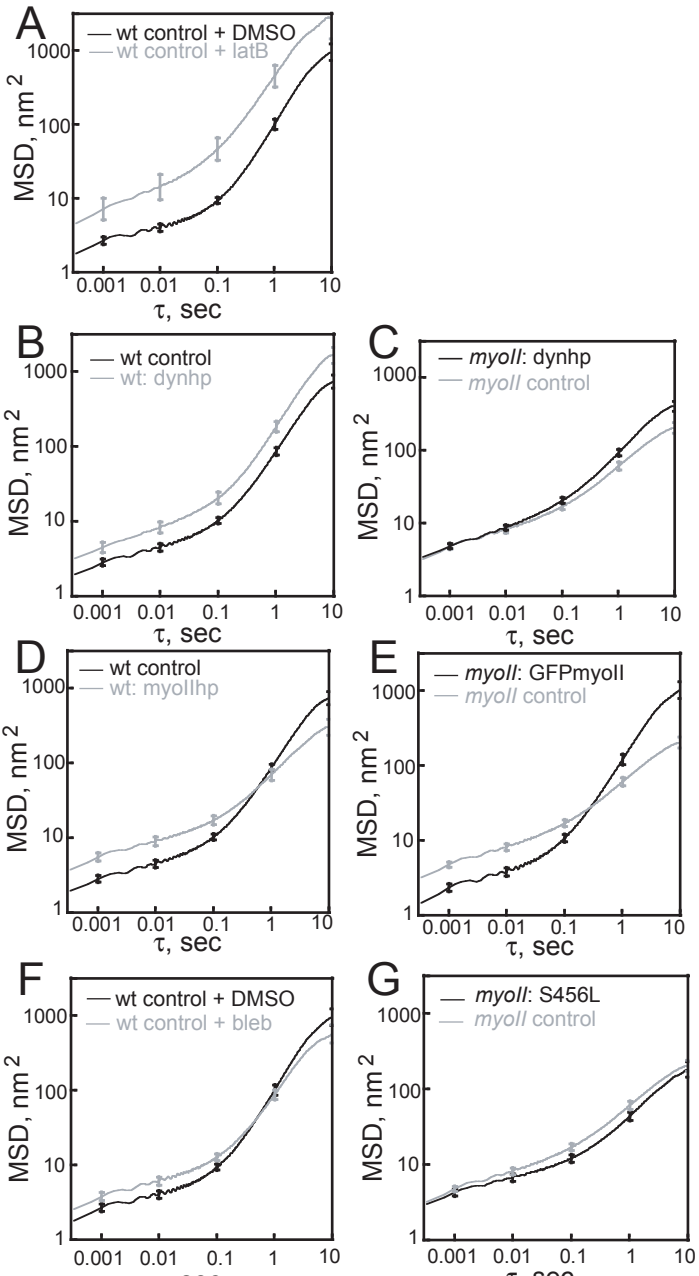
A
wt control + DMSO
wt control + latB
MSD, nm 2
τ, sec
B
wt control
wt: dynhp
C
myoII: dynhp
myoII control
D
wt control
wt: myoIIhp
E
myoII: GFPmyoII
myoII control
F
wt control + DMSO
wt control + bleb
G
myoII: S456L
myoII control

Figure 6

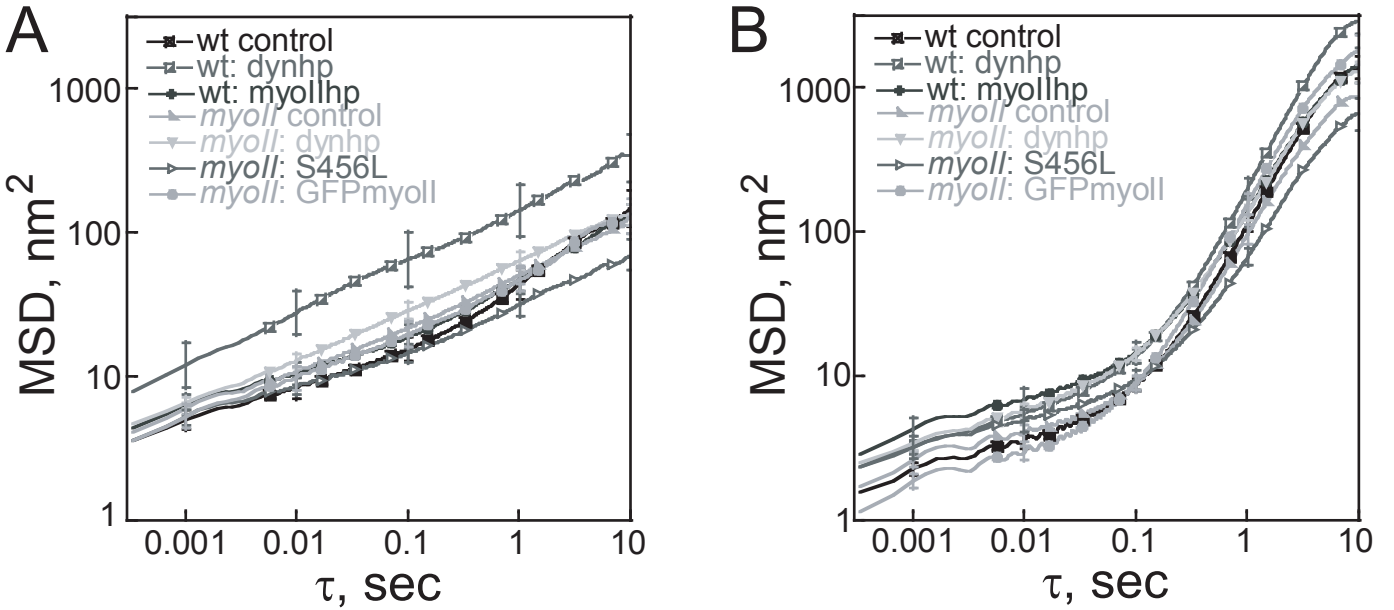
A
wt control
wt: dynhp
wt: myoIIhp
myoII control
myoII: dynhp
myoII: S456L
myoII: GFPmyoII
MSD, nm2
1000
100
10
1
0.001
0.01
0.1
1
10
τ, sec
B
wt control
wt: dynhp
wt: myoIIhp
myoII control
myoII: dynhp
myoII: S456L
myoII: GFPmyoII
MSD, nm2
1000
100
10
1
0.001
0.01
0.1
1
10
τ, sec

Figure 7